



ELSEVIER

Available online at www.sciencedirect.com

SCIENCE @ DIRECT®

Microelectronic Engineering 82 (2005) 189–195

MICROELECTRONIC
ENGINEERING

www.elsevier.com/locate/mee

Characterization of electroplated copper self-annealing with investigations focused on incorporated impurities

M. Stangl^{*}, J. Acker, V. Dittel, W. Gruner, V. Hoffmann, K. Wetzig

Leibniz Institute for Solid State and Materials Research, IFW Dresden, P.O. Box 27 01 16, D-01171 Dresden, Germany

Received 16 June 2005; accepted 22 July 2005
Available online 18 August 2005

Abstract

At room temperature electroplated copper exhibits changes in microstructure widely known as self-annealing. To investigate this phenomenon we simultaneously determined resistivity, residual stress, microstructure evolution, and behavior of organic impurities in three Cu layers of 600, 1000, and 2000 nm thickness. The examination of Cu layer impurities presupposed an extensive work of identification and elimination of contamination sources. After developing and applying several cleaning procedures it was possible to qualify and quantify incorporated C as indicator for organic impurities. The investigation of Cu self-annealing led to the conclusion that the microstructure evolution has to be divided into two periods. The first period of inhibited grain growth shows an impurity diffusion out of the metallization layer combined with a significant stress relaxation. In the following second period a forced grain growth evolution starts forming up a coarse grain microstructure.

© 2005 Elsevier B.V. All rights reserved.

PACS: 61.72.Ss; 66.30.Jt; 68.35.Dv; 81.15.Pq; 82.45.Vp; 83.85.St; 85.40.Ls

Keywords: Electrochemical deposition; Copper; Self-annealing; Additives; Stress; Impurity diffusion; GD-OES

1. Introduction

The electrochemical deposition of Cu is widely used for the preparation of metallization layers and to fill vias and trenches with high aspect ratio

in damascene process [1,2]. Electroplated Cu films have been reported to show an abnormal grain growth immediately after deposition described as self-annealing. This phenomenon of a significant microstructure evolution at room temperature is proved by many investigations documenting changes in resistivity, residual stress, grain growth, and texture [3–5]. It is supposed that self-annealing may strongly depend on the amount of additives

^{*} Corresponding author. Tel.: +49 351 4659 760; fax: +49 351 4659 452.

E-mail address: m.stangl@ifw-dresden.de (M. Stangl).

given to the plating solution [6]. Additives are organic and inorganic substances in the electrolyte in order to achieve uniform and homogeneous plating, fine grains, and void-free trench filling [7]. During electroplating additives and/or their corresponding breakdown products are capable to adsorb on the cathodic substrate and incorporate in the deposit [8–10]. It is supposed that impurities are embedded mainly into the free volume between the grains. Shimizu et al. [11] appreciates the possible amount of impurities far less than 1 wt%. Using low energy ion scattering and thermal desorption analysis Brongersma et al. [12] supposed an impurity segregation into the grain boundaries and a diffusion out to the Cu layer surface during self-annealing grain growth.

However, all previous investigations only state out a phenomenological examination of Cu self-annealing process. Particularly, the incorporation and degradation of Cu impurities is neither exactly clarified nor correctly understood. Though, the first successful qualification and quantification of impurities in thin electroplated Cu films by analytical radio frequency glow discharge optical emission spectrometry (RF-GD-OES) [13] prepared the basis for further extensive investigations. The quantification of C incorporation was an enormous challenge and demanded intensive preparatory work to reduce the RF-GD-OES detection limit. Based on the developed analytical methods the aim of the present work was to find fundamental driving forces for the phenomena of Cu self-annealing focused on differently thick metallization layers.

2. Experimental

For this study, we used thermally oxidized 3 inch Si(100) blanket wafers. First, a 50 nm Ta layer, which acts as a diffusion barrier for highly diffusive Cu atoms, and a 50 nm Cu seed layer were deposited by magnetron-sputtering (PVD, physical vapor deposition) without vacuum break. The electrochemical deposition was performed using a FIBRoplate™ IKo™ plating station (ECSI FIBRtools Company, Denville, NJ, USA) for horizontal plating (Fig. 1). The electrolyte solution

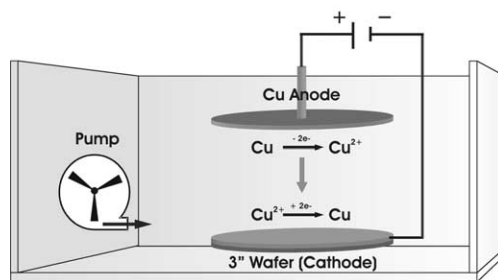


Fig. 1. Scheme of the electrochemical deposition.

contained a typical composition [14–16] of 0.25 M $\text{CuSO}_4 \cdot 5\text{H}_2\text{O}$, 1.8 M H_2SO_4 and 1.41 mM Cl^- in form of KCl (all chemicals p.A., Merck, Germany). A prescribed amount of two commercially available additives SC MD and SC LO 70/30 (Enthone Inc., Germany) was admixed. A pump circulated the electrolyte and a dc current density of 15 mA cm^{-2} was applied to generate electroplated Cu films.

Immediately after deposition, stress was determined by laser-optical wafer-curvature measurements (Flexus, Tencor Instruments). Simultaneously, the behavior of resistivity could be monitored by an in-house fabricated four-point probe resistivity measuring system. Focused ion beam (FIB) analyses were carried out with a FIB200 (FEI Company) to examine the grain growth evolution. The advantage of FIB imaging is the high grain orientation contrast as a result of a strong channelling effect of the Ga ions. The linear grain size of surface etched Cu metallizations was determined by chord length analysis and imaged using scanning electron microscopy (LEO Gemini 1530).

Incorporated carbon in electroplated Cu metallizations was determined by RF-GD-OES (LECO SDP-750, rotary vacuum pump with Al_2O_3 sorbent). Secondary ion mass spectrometry (SIMS) (PHI 6300 based system, 3.5 kV Cs^+ primary ion source) confirmed the RF-GD-OES results. C was quantified by matrix independent calibration with iron based NIST standards and the sputtered craters were measured using an optical depth profilometer (FRT, MicroProf) for calculating the sputtering rate. One basic requirement for good qualitative and quantitative analyses was a

sufficiently cleaned sample surface. Pure hydrogen peroxide (H_2O_2 , 30%) was used for oxidation and low concentrated sulfuric acid (H_2SO_4 , 5%) for the removal of the oxidized and contaminated surface of about 40 nm thickness. After cutting the 3 in. coated wafer into small samples of $1 \times 1 \text{ cm}^2$ residual stress and resistivity were continuously measured. The remaining samples were used for RF-GD-OES examinations carried out in 1 h time intervals until the end of self-annealing indicated by a resistivity drop of $\approx 20\%$.

3. Results and discussion

Resistivity is the most important global parameter for documenting the progress of self-annealing. The change in resistivity is closely connected to microstructure evolution. The relation between microstructure and resistivity is exemplarily shown in Fig. 2 for a 1000 nm Cu layer over 40 h after deposition. Within the first 10 h after electroplating, grain growth seems to be inhibited and resistivity shows a significant incubation time with a little decrease of about 2%. In the following 30 h

a forced microstructure evolution starts and the initial grains with an as-deposited grain size of less than 100 nm grew into larger grains of several micrometers in diameter. In this period, resistivity decreases about 18% as a result of lower electron grain boundary scattering in accordance to the Mayadas–Shatzkes model [17,18].

Subsequent to the typical documentation of self-annealing at our samples we were interested in the behavior of organic impurities in the Cu metallization during this period. To improve the RF-GD-OES detection limit of C a basic requirement is a long pre-sputtering with thermally cleaned Si samples. Pre-sputtering of $\approx 0.5 \text{ h}$ is necessary to burn down impurities adsorbed inside the glow discharge source. The enormous decrease of C detection limit is illustrated by depth profiles of thermally cleaned Si samples (Fig. 3(a)). It shows, that adsorbed impurities falsify the C detection, not only near the surface but also in the total depth profile.

Furthermore, some of the organic compounds in the plating bath have a strong surfactant character and adhere to the wafer surface when the wafer is removed from the bath (Langmuir–Blodgett

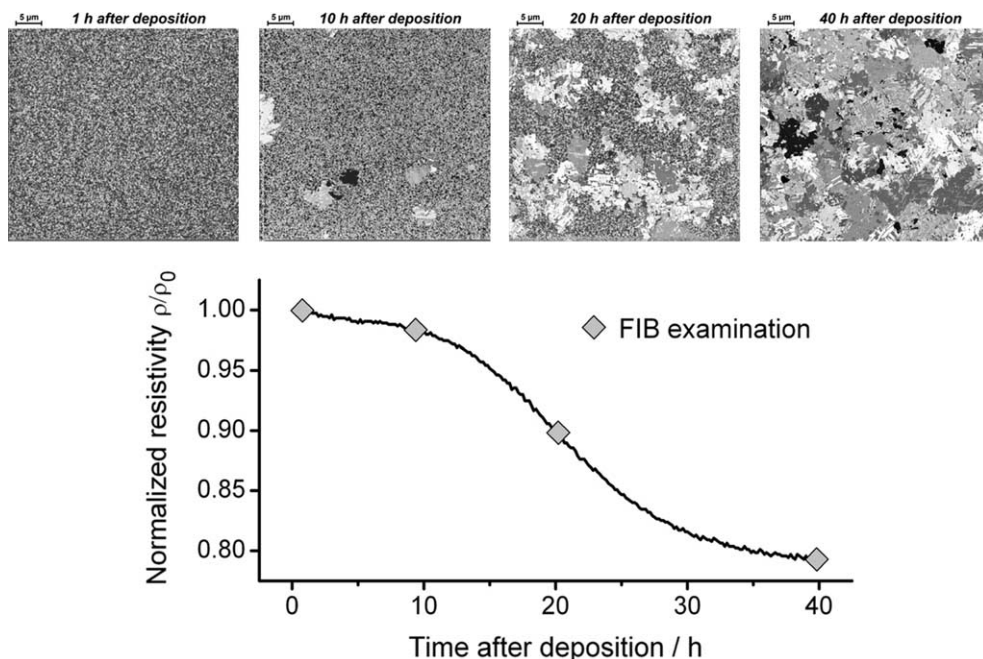


Fig. 2. Resistivity and microstructure evolution during self-annealing of a 1000 nm Cu layer.

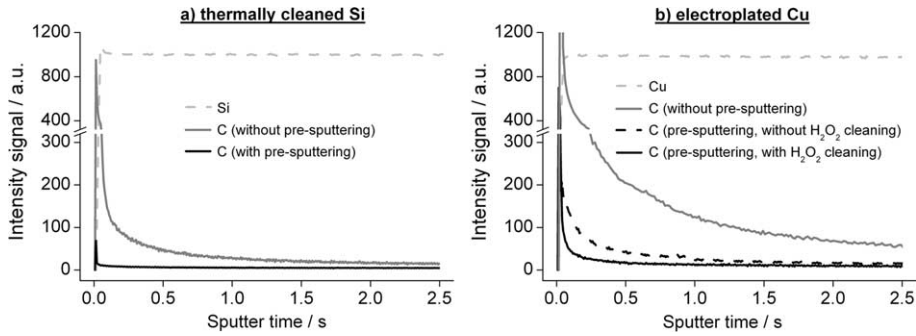


Fig. 3. RF-GD-OES depth profiles of thermally cleaned Si (a) and electroplated Cu (b) depending on different cleaning procedures.

film). Several cleaning procedures were tested and H_2O_2 conditioning in combination with a subsequent H_2SO_4 etching yield the best effect to remove the surface contamination [13]. In addition, before each RF-GD-OES measurement the particular sample was pre-cleaned in H_2O_2 again and dried by a nitrogen gas stream. The success of the extensive cleaning efforts is illustrated for electroplated Cu samples (Fig. 3(b)).

It turned out, that the pre-sputtering procedure is more effective to reduce C contaminations than the wet cleaning process using H_2O_2 and H_2SO_4 . Therefore, system-dependent GD source contamination is the major factor in falsifying RF-GD-OES depth profiles. The fully reproducible C signal of thermally cleaned Si is considered as detection limit for C RF-GD-OES measurements. For quantitative analysis this C signal is subtracted from C signals in measured Cu films. The 0.5 h pre-sputtering has to be done before each measurement to ensure the reproducibility of RF-GD-OES analyses.

Fig. 4 shows four carbon depth profiles of a 1000 nm Cu metallization between 1 and 10 h. The significant gradient towards the Cu layer surface and the remarkable decrease of incorporated C species probates the hypothesis of a strong diffusion of organic impurities out of the metallization. Particularly, the shoulder in the C intensity curves near the surface support this assumption and indicates a diffusion-limiting surface process. The C diffusion is assumed to proceed already with the Cu deposition because C depth profiles show no equal distribution even short time after electroplating. SIMS measurements performed with the same

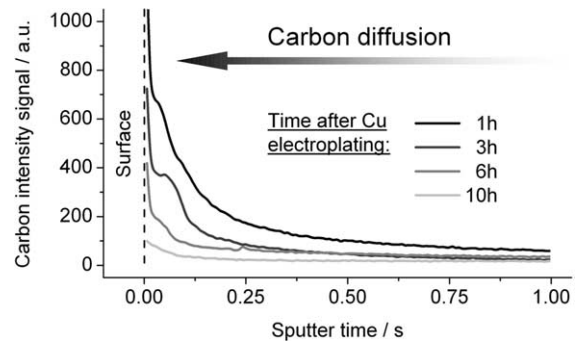


Fig. 4. Carbon RF-GD-OES depth profiles of 1000 nm Cu films at different times after electroplating.

electroplated Cu layers confirmed the qualitative curve shapes and C diffusion.

For C quantification a matrix independent calibration was carried out using iron based NIST standards 1761–1767. The C content specific RF-GD-OES intensity signal was determined 150 s after the start of sputtering and follows the equation,

$$I(C) = EY \cdot SR \cdot c(C) + I_{\text{Background}}, \quad (1)$$

where $I(C)$ is the C intensity of standard/V, EY is the emission yield/ $\text{V s } \mu\text{g}^{-1}$, SR is the sputtering rate/ $\mu\text{g s}^{-1}$, and $c(C)$ is the C content in standard/ $\mu\text{g g}^{-1}$. According to Eq. (1) the sputtered mass per time of C ($dm(C)/dt/\mu\text{g s}^{-1}$) is proportional to the measured intensity.

$$\frac{dm(C)}{dt} = SR \cdot c(C). \quad (2)$$

The SR of all NIST standards were measured and the C intensities were plotted in dependence on $dm(C)/dt$. The slope of this curve is equal to the

EY which is matrix independent for constant electrical discharge conditions. The per time sputtered mass of C in a Cu and Fe matrix is calculated by Eq. (1) because both matrices deliver the same current at equal constant high frequency voltage and pressure. Now, the C intensity of NIST standards and all discrete C intensities of sputtered Cu samples in a discrete sputter time interval dt are converted to a C mass m_x . According to Eq. (3) the accumulated measured discrete C masses m_x deliver the C content m_C of the whole sputtered sample volume. The integration time t (s) is determined between the start of sputtering and the increase of Ta intensity signal indicating the reached diffusion barrier,

$$m_C = \sum_1^n m_x, \tag{3}$$

$$m_C = \int_0^t \frac{(I(C) - I_{\text{Background}})}{EY} \cdot dt$$

Using the crater diameter and the Cu layer thickness, e.g. investigated by FIB analyses, for determining the sputtered Cu volume ($V_{\text{Cu}} = 1/4\pi d^2 \cdot h$) Eq. (4) is able to calculate the C content $c_{\text{C(sample)}}$ in the electroplated Cu film

$$c_{\text{C(Sample)}} = \frac{m_C}{m_{\text{Sample}}} = \frac{m_C}{m_{\text{Cu}}} \quad \text{with}$$

$$m_{\text{Sample}} = m_{\text{Cu}} \quad \text{if } m_{\text{Impurities}} \ll m_{\text{Cu}} \tag{4}$$

$$c_{\text{C(Sample)}} = \frac{m_C}{\rho_{\text{Cu}} \cdot V_{\text{Cu}}}$$

where $c_{\text{C(Sample)}}$ is the C content in sputtered sample/ $\mu\text{g g}^{-1}$, m_{Sample} is the mass of sputtered

sample/g, m_C is the mass of sputtered C/g, m_{Cu} is the mass of sputtered Cu/g, ρ_{Cu} is the Cu density/ g cm^{-3} and V_{Cu} is the sputtered Cu volume/ cm^{-3} .

Carbon content (Fig. 5(a)), residual stress (Fig. 5(b)) and resistivity (Fig. 5(c)) were continuously measured during self-annealing of 600, 1000, and 2000 nm Cu layers. Fig. 5(a) illustrates a decreasing C content immediately after deposition joined with a migration of organic impurities towards the Cu layer surface for all Cu metallizations. Remarkably, the thicker the Cu layer the faster is the diffusion. For 2000 nm Cu this impurity diffusion is finished within the first hour after deposition presumably supported by the higher initial stress. The comparison of all Cu layers shows an increase of C degradation with increasing initial stress. Hence, initial stress is assumed as an important precondition for a fast impurity diffusion. After finished stress relaxation all Cu layers reach an almost stress-free stage. The oscillations in the stress–time curves were caused by temperature fluctuations. Wendrock et al. [19] explained the stress relaxation as a consequence of a reduced defect volume and an increase in density of the material. Obviously, the end of stress relaxation correlates with the end of incubation time and the starting step decrease in resistivity of $\approx 20\%$.

The presented results emphasize the inference that impurity diffusion and stress relaxation lead to the incubation time of inhibited grain growth and represent the necessary preconditions for a forced microstructure evolution observed by the resistivity drop terminating the self-annealing process.

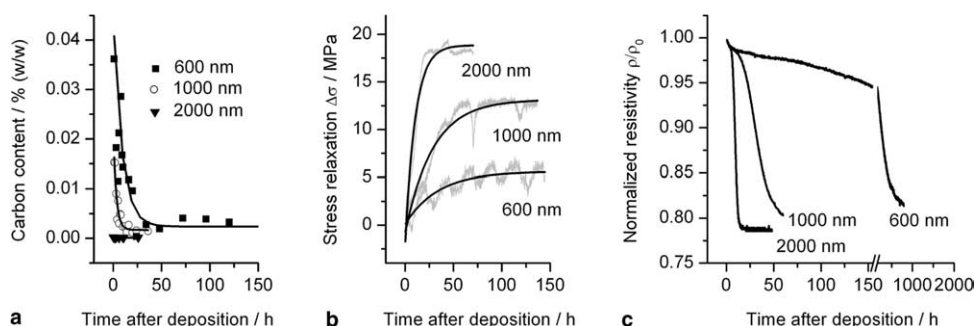


Fig. 5. Carbon content (a), stress relaxation (b), and resistivity behavior (c) of 600, 1000, and 2000 nm Cu metallization layers after electroplating.

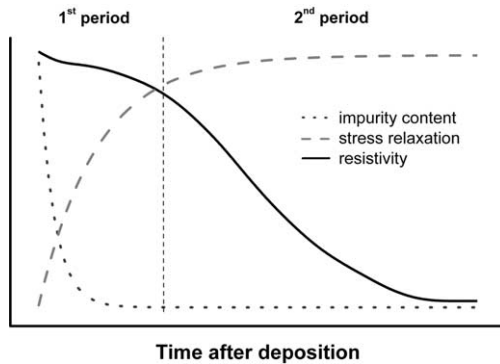


Fig. 6. General relation between impurity degradation, stress relaxation, and decreasing resistivity.

4. Conclusion

The labor-intensive identification and elimination of contamination sources serve as requirement for precise RF-GD-OES measurements. Thereby, it was possible to investigate and quantify the C content in electroplated Cu layers. Because C indicates incorporated organic impurities the behavior of these impurities could be determined during self-annealing. Three metallizations with 600, 1000, and 2000 nm electroplated Cu were investigated to display the dependency of self-annealing on the layer thickness. During self-annealing all examined Cu layers showed a significant change in resistivity. Remarkably, the resistivity curves can be subdivided into two periods illustrated in Fig. 6. The first period describes an incubation time of inhibited grain growth. During incubation time organic impurities degrade and diffuse towards the metallization surface to leave the Cu layer. Simultaneously, residual stress reaches an almost stress-free stage by stress relaxation. The comparison of impurity degradation and stress relaxation leads to the conclusion that a higher initial stress forces a faster diffusion. The reached stress-free stage marks the beginning of the second period of accelerated grain growth. This microstructure evolution is indicated by a steep decrease in resistivity of 20% on average and implies a completion of the self-annealing process.

Recapitulating, these studies might be a contribution for a deeper understanding of mechanisms

and fundamental driving forces for the self-annealing of differently thick electroplated Cu layers. Significant preconditions were determined explaining the irregular grain growth during Cu self-annealing leading to stress-free, large grained, and very pure Cu metallizations for semiconductor interconnects.

Acknowledgements

The authors thank S. Oswald for the excellent SIMS analyses and S. Strehle for supporting the stress measurements. The authors are also appreciated to R. Kaltofen for manufacturing the Si(100) samples with Ta barrier and Cu seed layer. Furthermore, the collaboration with H. Wendrock and S. Menzel regarding to the FIB work and resistivity experiments is acknowledged gratefully.

References

- [1] K. Wetzig, C.M. Schneider, *Metal Based Thin Films for Electronics*, vol. 1, Wiley-VCH, 2003, ISBN 3-527-40365-5.
- [2] P.C. Andricacos, C. Uzoh, J.O. Dukovic, J. Horkans, H. Deligianni, *Electrochem. Microfab.* 42 (5) (1998) 567–574.
- [3] S. Lagrange, S.H. Brongersma, M. Judelewicz, A. Saerens, I. Vervoort, E. Richard, R. Palmans, K. Maex, *Microelectr. Eng.* 50 (2000) 449–457.
- [4] W.H. The, L.T. Koh, S.M. Chen, J. Xie, C.Y. Li, P.D. Foo, *Microelectr. J.* 31 (2001) 579–585.
- [5] S.H. Brongersma, E. Kerr, I. Vervoort, K. Maex, *Proc. AIP Conf.*, Melville, NY 612 (2002) 229–234.
- [6] M.S. Yoon, Y.J. Park, Y.C. Joo, *Thin Solid Films* 408 (2002) 230–235.
- [7] L.T. Koh, G.Z. You, C.Y. Li, P.D. Foo, *Microelectr. J.* 33 (2002) 229–234.
- [8] L. Bonou, M. Eyraud, R. Denoyel, Y. Massiani, *Electrochim. Acta* 47 (2002) 4139–4148.
- [9] T.P. Moffat, J.E. Bonevich, W.H. Huber, A. Stanishevsky, D.R. Kelly, G.R. Stafford, D. Josell, *J. Electrochem. Soc.* 147 (12) (2000) 4524–4535.
- [10] M. Tan, J.N. Harb, *J. Electrochem. Soc.* 150 (6) (2003) C420–C425.
- [11] K. Shimizu, N. Kasahara, H. Habazaki, P. Skeldon, G.E. Thompson, *Surf. Interf. Anal.* 35 (2003) 611–617.
- [12] S.H. Brongersma, E. Kerr, I. Vervoort, A. Saerens, K. Maex, *J. Mater. Res.* 17 (2002) 582–589.
- [13] M. Stangl, V. Dittel, J. Acker, V. Hoffmann, W. Gruner, S. Strehle, K. Wetzig, *Appl. Surf. Science* (2005), in press.
- [14] M. Militzer, P. Freundlich, D. Bizzotto, *Mater. Sci. Forum* 467–470 (2004) 1339–1344.

- [15] T.P. Moffat, D. Wheeler, D. Jossell, *J. Electrochem. Soc.* 151 (2004) C262–C271.
- [16] S. Miura, H. Honma, *Surf. Coat. Technol.* 169–170 (2003) 91–95.
- [17] A.F. Mayadas, M. Shatzkes, *Phys. Rev. B* 1 (4) (1970) 1382–1389.
- [18] J.M.E. Harper, C. Cabral, P.C. Andricacos, L. Gignac, I.C. Noyan, K.P. Rodbell, C.K. Hu, *J. Appl. Phys.* 86 (1999) 2516–2524.
- [19] H. Wendrock, W. Brueckner, M. Hecker, T.G. Koetter, H. Schloerb, *Microelectr. Rel.* 40 (2000) 1301–1304.